Energetics of the Native Energy Landscape of a Two-Domain Calcium Sensor Protein: Distinct Folding Features of the Two Domains†

Sulakshana Mukherjee, P. M. Krishna Mohan, Kavita Kuchroo, and Kandala V. R. Chary*

Department of Chemical Sciences, Tata Institute of Fundamental Research, Homi Bhabha Road, Mumbai 400 005, India

Received March 9, 2007; Revised Manuscript Received June 1, 2007

ABSTRACT: The protein folding energy landscape allows a thorough understanding of the protein folding problem which in turn helps in understanding various aspects of biological functions. Characterizing the cooperative unfolding units and the intermediates along the folding funnel of a protein is a challenging task. In this paper, we investigated the native energy landscape of *Eh*CaBP, a calcium sensor, belonging to the same EF-hand superfamily as calmodulin. *Eh*CaBP is a two-domain EF-hand protein consisting of two EF-hands in each domain and binding to four Ca^{2+} cations. Native-state hydrogen exchange (HX) was used to assess the folding features of the landscape and also to throw light on the structure-folding function paradigm of calcium sensor proteins. HX measurements under the EX2 regime provided the thermodynamic information about the protein folding events under native conditions. HX studies revealed that the unfolding of *Eh*CaBP is not a two-state process. Instead, it proceeds through cooperative units. The C-terminal domain exhibits less denaturant dependence than the N-terminal domain, suggesting that the former is dominated by local fluctuations. It is interesting to note that the N- and C-terminal domains of *Eh*CaBP have distinct folding features. In fact, these observed differences can regulate the domain-dependent target recognition of two-domain Ca^{2+} sensor proteins.

Calcium is one of the most commonly used ions in a multitude of biological processes. It triggers new life during fertilization and controls several developmental processes. The cellular processes in which it is involved include metabolism, proliferation, secretion, contraction, learning, memory, cell death, etc. (*1*−*8*). In all these processes, Ca^{2+} interacts with a variety of proteins. The proteins that bind to Ca^{2+} are called calcium binding proteins (CaBPs)[1] (*9*). EF-hand CaBPs (EF-CaBPs) constitute a growing superfamily of CaBPs (*10*−*13*). EF-hand in these proteins represents a canonical Ca^{2+} binding motif, which consists of a contiguous 12-residue loop flanked by two helices (*14*, *15*). The EF-CaBPs are broadly divided into Ca^{2+} sensors and Ca^{2+} buffers. Ca^{2+} sensors such as calmodulin (CaM), troponin C (TnC), etc. (*16*−*20*), undergo huge conformational changes upon binding to Ca^{2+}. On the other hand, the Ca^{2+} buffers such as calbindin D_{9k} (*21*−*23*) undergo modest conformational changes upon Ca^{2+} binding. In Ca^{2+} sensors, binding of Ca^{2+} opens the EF-hand, thereby exposing the buried hydrophobic surface to the solvent. The exposed hydrophobic surface now binds to the target peptides and proteins, leading to further conformational change (*16*, *24*). The protein in its Ca^{2+}-bound form needs to undergo various conformational readjustments through different folding or unfolding events to perform several functional activities. Hence, it is important to explore the energetics of the folding−unfolding pathway of the Ca^{2+}-bound forms of this class of proteins to understand the conformational adaptability of Ca^{2+} sensor proteins, which is essential for their biological activity.

The energy landscape view of the protein folding process is generally described in terms of the folding funnel, in which the broad end represents the heterogeneous unfolded states while the narrow end represents the homogeneous native state (*25*−*27*). Different members of the ensemble may fold or unfold along different pathways, and hence, their energy profiles could be different. In the presence and absence of a denaturant, a protein can unfold or fold by various mechanisms. Some proteins have been shown to fold by a two-state mechanism without the accumulation of any intermediates, while others adopt a different mechanism that involves one or more intermediates (*28*−*31*). Thus, the complete analysis of any protein folding landscape is a challenging task.

The backbone amide hydrogen−deuterium exchange (HX) is one of the most promising techniques for exploring the protein folding landscape under native conditions (*32*−*35*). The HX is based on the fact that proteins continuously fold and unfold in solution. The exchange process takes place

† The facilities provided by the National Facility for High Field NMR, supported by the Department of Science and Technology (DST), the Department of Biotechnology (DBT), the Council of Scientific and Industrial Research (CSIR), and the Tata Institute of Fundamental Research, Mumbai, India, are gratefully acknowledged. S.M. and P.M.K.M. are recipients of the TIFR Alumni Association Scholarship (2003−2005) for career development and Sarojini Damodaran International Fellowship supported by the TIFR endowment fund.

* To whom correspondence should be addressed: Department of Chemical Sciences, Tata Institute of Fundamental Research, Homi Bhabha Road, Mumbai 400 005, India. Telephone: 91 22 22782489. Fax: 91 22 2280 4610. E-mail: chary@tifr.res.in.

[1] Abbreviations: NMR, nuclear magnetic resonance; HSQC, heteronuclear single-quantum coherence; CaBP, calcium binding protein; *Eh*CaBP, *Entamoeba histolytica* calcium binding protein; CaM, calmodulin; TnC, troponin C; EGTA, ethylene glycol bis(β-aminoethyl ether)-*N*,*N*′-tetraacetate; HX, hydrogen exchange; PUF, partially unfolded form; GdmCl, guanidine hydrochloride.

10.1021/bi700477h CCC: $37.00
Published on Web 08/08/2007

during the existence of the protein in the higher-energy unfolded conformations. The higher-energy unfolded conformations are populated according to the Boltzmann distribution and represent a small population of the system as a whole. Under the native conditions, at any instant of time, the equilibrium is always toward the folded state and only a very small fraction exists in the unfolded state. The native HX utilizes the advantage of the equilibrium between the native and unstable intermediate states and is highly useful in identifying various partially unfolded forms (abbreviated hereafter as PUFs) along the folding transition (*36*−*39*). The PUFs thus identified are typically higher in free energy, being ≥5 kcal/mol above the native state (*37*, *40*).

We have chosen a Ca^{2+} sensor from the protozoan *Entamoeba histolytica*, which is an etiologic agent of amoebiasis affecting millions worldwide (abbreviated hereafter as *Eh*CaBP), in its Ca^{2+}-bound form to study its unfolding landscape (*41*, *42*). *Eh*CaBP is a two-domain EF-hand protein consisting of two EF-hands in each domain and is known to be involved in the pathogenesis of amoebiasis (*42*). The Ca^{2+}-free form of the protein (apo-*Eh*CaBP) has been shown to adopt a partially collapsed structure, while the Ca^{2+}-bound form (holo-*Eh*CaBP) adopts an ordered structure (*42*, *43*). In both the apo and holo forms, it has been shown that the hydrophobic moieties are exposed on the surface of *Eh*CaBP, though the degree of exposure is 3−4-fold greater in the case of holo-*Eh*CaBP compared to that on the surface of apo-*Eh*CaBP. The folding process from apo- to holo-*Eh*CaBP is mainly governed by the affinity of the individual metal binding sites for the Ca^{2+} (*43*). In this study, we investigated the energetics of the native energy landscape of holo-*Eh*CaBP using native HX experiments. This study reveals that the two domains in *Eh*CaBP exhibit distinct folding features. The N-terminal domain exhibits a stronger denaturant dependence compared to the C-terminal counterpart. Further, the C-terminal domain is found to be more dominated by local fluctuations. This study provides a rationale for the structure−folding function paradigm of calcium sensor proteins.

MATERIALS AND METHODS

Theory of Hydrogen Exchange. For structurally protected hydrogens such as the backbone $^1H^N$ protons in proteins, the HX process can be considered as a two-state process (*44*, *45*), as in eq 1, with hydrogens that are either nonexchangeable in the protected state (NH_{closed}) or susceptible to exchange in some transiently open state (NH_{open}):

$$NH_{closed} \underset{k_{cl}}{\overset{k_{op}}{\rightleftharpoons}} NH_{open} \xrightarrow{k_{rc}} \text{exchanged} \quad (1)$$

where k_{op} is the opening rate, k_{cl} is the closing rate, and k_{rc} is the intrinsic exchange rate of the $^1H^N$. Under steady-state conditions, the exchange rate k_{obs} determined by eq 1 is given by eq 2 (*44*, *45*).

$$k_{obs} = \frac{k_{op}k_{rc}}{k_{op} + k_{cl} + k_{rc}} \quad (2)$$

Under native conditions where $k_{op} \ll k_{cl}$, the observed exchange rate (k_{obs}) can be given as follows (*44*):

$$k_{obs} = \frac{k_{op}k_{rc}}{k_{cl} + k_{rc}} \quad (3)$$

Under EX2 (bimolecular exchange) conditions where $k_{cl} \gg k_{rc}$ (low pH and temperature), the exchange rate becomes

$$k_{obs} = k_{rc}\left(\frac{k_{op}}{k_{cl}}\right) \quad (4)$$

The stabilization free energy of the protecting structure can thus be calculated as

$$\Delta G_{HX} = -RT \ln\left(\frac{k_{op}}{k_{cl}}\right) = -RT \ln K_{op} \quad (5)$$

where K_{op} is the equilibrium constant of the unfolding, R is the universal gas constant, and T is the absolute temperature.

In proteins, the $^1H^N$ may undergo HX via global unfolding (uf), local fluctuation (lf), or both (*29*). Individual contributions of the free energy of unfolding (ΔG_{uf}) and free energy of local fluctuation (ΔG_{lf}) can be obtained for each probed residue according to the equation

$$\Delta G_{HX} = -RT \ln(K_{uf} + K_{lf}) \quad (6)$$

where $K_{uf} = e^{[(m[GdmCl] - \Delta G_{uf})/(RT)]}$ and $K_{lf} = e^{[-\Delta G_{lf}/(RT)]}$. Here m represents the denaturant dependence of the unfolding free energy.

Protein Expression and Purification. The overexpression and purification of *Eh*CaBP in its Ca^{2+}-bound and Ca^{2+}-free forms were carried out as described previously (*42*, *43*, *46*). All labeled chemicals used were from either Cambridge Isotope Laboratories or Spectra Stable Isotopes (Spectra Gases Inc.). Other required chemicals were of ultrapure grade from Sigma-Aldrich and SRL. The purity and yield of the protein in the eluted fractions were confirmed by 15% SDS−PAGE and matrix-assisted laser desorption ionization time-of-flight (MALDI-TOF) mass spectrometry. The fractions were collected and concentrated by ultrafiltration for NMR and other biophysical studies. The concentration of the purified protein was determined by measuring the absorbance at 280 nm. Deuterated guanidine hydrochloride (GdmCl) was used for all the studies performed with CD and NMR.

Circular Dichroism. The stability of holo-*Eh*CaBP was studied against a chemical denaturant like GdmCl at pH 7.0 in ^2H_2O and at 20 °C. The concentration of the GdmCl was varied from 0 to 8.3 M. The stability was determined by monitoring the molar ellipticity (θ) at 222 nm as a function of GdmCl concentration. Protein samples at a concentration of 10 μM (50 mM Tris and 5 mM $CaCl_2$) were used for the unfolding experiments. The experiments were repeated thrice with a fresh batch of protein samples, and the thermodynamic parameters that were obtained were found to be similar.

The GdmCl-induced unfolding of *Eh*CaBP was analyzed and fitted to the linear extrapolation model with an assumption of two-state unfolding (*47*). The baselines before (Y_N) and after (Y_U) the unfolding were assumed to be straight lines, where k_N and k_U are the slopes, b_N and b_U are the intercepts, and [D] is the denaturant concentration. The free energy toward unfolding by GdmCl, ΔG_{NU}, is assumed to obey the linear equation

$$\Delta G_{NU} = \Delta G_{NU}(H_2O) - m_D[D] \quad (7)$$

where $\Delta G_{NU}(H_2O)$ is the unfolding free energy at a zero denaturant concentration and m_D is the influence of denaturant concentration on stability.

The GdmCl concentration at the transition midpoint (C_m) was calculated from the above equation by setting ΔG_{NU} to zero. The errors in the reported values of the different parameters were estimated to one standard deviation. The standard deviations were obtained directly from the fitting procedures. The data were normalized according to

$$F_{app} = \frac{Y_O - Y_N}{Y_U - Y_N} \quad (8)$$

Y_N and Y_U hence correspond to the ellipticity of the native and Y_O is the observed ellipticity at given denaturant concentration, respectively, as a function of GdmCl concentration and fitted to

$$F_{app} = \frac{e^{-[\Delta G_{NU}(H_2O) - m_D[D]]/(RT)}}{1 + e^{-[\Delta G_{NU}(H_2O) - m_D[D]]/(RT)}} \quad (9)$$

where R is the molar gas constant and T is the absolute temperature.

NMR Spectroscopy. NMR experiments were carried out on a Varian *INOVA* 600 MHz NMR spectrometer equipped with a pulsed field gradient unit and triple-resonance probe with an actively shielded Z-gradient, operating at a ^{1}H frequency of 599.862 MHz. Sensitivity-enhanced two-dimensional (2D) ^{15}N−^{1}H heteronuclear single-quantum correlation spectra (HSQC) (*48*) of the protein sample (pH 7.0 and 20 °C) containing 50 mM Tris and 5 mM $CaCl_2$ were recorded with the ^{1}H offset placed on the H_2O resonance at 4.78 ppm and the ^{15}N offset at 123.8 ppm. During the course of all experiments, the protein samples were found to be stable and did not change or degrade with time. ^{1}H chemical shifts were calibrated relative to 2,2-dimethyl-2-silapentane-5-sulfonate (DSS). Spectra were processed using VNMR 6.1B (Varian) and Felix 2002 (Molecular Simulations Inc.). The 2D ^{15}N−^{1}H HSQC data were typically apodized using a 90° phase-shifted sine square-bell window function along both the dimensions before zero-filling and 2D Fourier transformation. Integral volumes (in arbitrary units) for the individual ^{15}N−^{1}H cross-peaks in these spectra were measured using Felix 2002 (Accelrys).

Hydrogen Exchange Studies. The protein samples were lyophilized after the pH of the solution to was adjusted to 7.0. HX was initiated by dissolving the lyophilized samples in ^2H_2O, and the pDs were measured. The reported pD is the corrected pH obtained by the addition of 0.4 unit to the measured pH value after the sample is dissolved in ^2H_2O. The samples were loaded on a pretuned and preshimmed NMR spectrometer, and a series of 35−40 ^{15}N−^{1}H HSQC spectra were recorded at different time intervals (for ~2 months) depending on the rate of decay. Each ^{15}N−^{1}H HSQC spectrum was recorded for a period of 20 min and consisted of 128 complex increments in the indirect ^{15}N dimension. Similarly, the experiments were carried out under the subdenaturing conditions at various GdmCl concentrations. The GdmCl concentrations used were 0.1, 0.2, 0.3, 0.4, 0.5, 0.75, 1.0, 1.5, 2.0, and 2.5 M. The above-mentioned procedure involving lyophilization did not have any adverse effect on the protein sample. The HX rates of individual $^1H^N$ in *Eh*CaBP were measured by monitoring the $^1H^N$ decays by integrating the volumes of the nonoverlapping peaks. The decay of the individual peak volumes was fitted to the single-exponential decay function. K_{op} was then calculated using the equation $K_{op} = k_{obs}/k_{rc}$, where k_{rc} is theoretically determined for a residue in a specific tripeptide context (*49*). The free energy of HX (ΔG_{HX}) is obtained using eq 5. ΔG_{uf}, ΔG_{lf}, and the m values were obtained by fitting the plot of ΔG_{HX} versus GdmCl concentration to eq 6. Here, ΔG_{uf} denotes the unfolding free energy extrapolated to 0 M GdmCl.

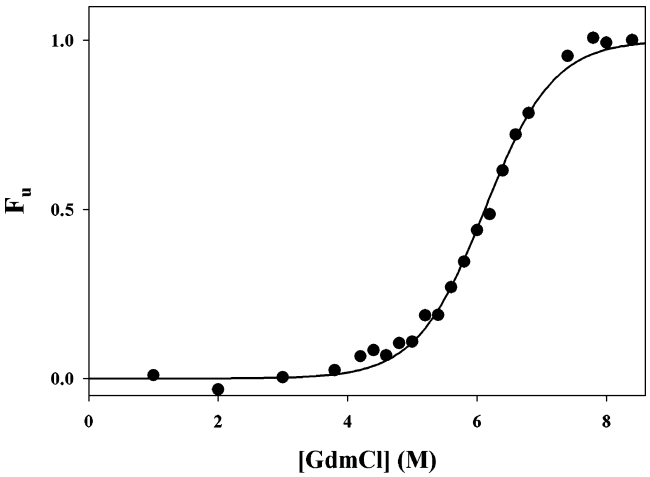

FIGURE 1: Equilibrium unfolding of Ca^{2+}-bound *Eh*CaBP vs [GdmCl] at pD 7.4 as measured by circular dichroism at 222 nm. The ΔG_u that was obtained was 6.8 ± 0.3 kcal/mol, and the m value was 1.1 ± 0.1 kcal mol^{-1} M^{-1}. The solid line is the best fit obtained using the equations for a two-state model as described in Materials and Methods.

RESULTS

Global Unfolding Behavior of EhCaBP. The global unfolding of holo-*Eh*CaBP was monitored by using far-UV CD spectroscopy at 222 nm against GdmCl concentration (pD 7.4 in ^2H_2O) (Figure 1), and the unfolding energy (ΔG_{uf}) was obtained as mentioned in Materials and Methods. Denaturation studies using CD were carried out essentially to correlate the unfolding energies obtained here with those of HX studies discussed below. For this purpose, both denaturations using CD and HX studies were performed in 100% ^2H_2O since it is known that the bulk solvent has a variable effect on protein stability (*50*). The global energies of unfolding (ΔG_{uf}) by CD in ^2H_2O (Figure 1) and H_2O (data not shown) are found to be 6.8 ± 0.3 and 6.4 ± 0.4 kcal/mol, respectively. This suggests that the bulk solvent effect on *Eh*CaBP is minimal. The m value which describes the denaturant dependence of the free energy change between two states, derived by fitting the data to a two-state model (Figure 1), is found to be small (1.1 ± 0.1 kcal mol^{-1} M^{-1} at pD 7.4). This indicates a low cooperativity of transition from a folded state to an unfolded one.

Native-State Hydrogen Exchange Studies on EhCaBP. Native-state hydrogen exchange (HX) is one of the most powerful techniques for probing the energetics of the folding landscape. To understand the thermodynamics of unfolding at the residue level and the nature of the energy landscape of the folding transition of *Eh*CaBP, we performed native-

Table 1: Summary of the Various Thermodynamic Parameters Obtained for the Individual Residues[a]

residue	EF-hand	ΔG_{HX} (kcal/mol)	*m* value (kcal mol^{-1} M^{-1})	ΔG_{uf} (kcal/mol)	ΔG_{lf} (kcal/mol)	class
Ile 9	I	4.5	0.96 ± 0.32	5.59 ± 0.60	4.49 ± 0.14	III
Val 11	I	6.8	1.49 ± 0.07	6.59 ± 0.06	–	II
Asp 14	I	6.8	2.37 ± 0.17	6.71 ± 0.07	–	II
Ala 16	I	8.6	2.24 ± 0.08	8.48 ± 0.05	–	II
Ser 18	I	8.0	2.44 ± 0.56	7.70 ± 0.17	–	II
Val 22	I	8.6	2.47 ± 0.08	8.64 ± 0.08	–	II
Lys 23	I	7.1	2.23 ± 0.39	8.29 ± 0.48	7.05 ± 0.16	III
Ala 24	I	6.2	0.56 ± 0.05	6.09 ± 0.05	–	II
Phe 25	I	ND[b]	1.68 ± 0.14	7.73 ± 0.13	–	II
Val 26	I	ND[b]	3.29 ± 0.19	8.11 ± 0.15	7.51 ± 0.15	III
Leu 40	II	5.6	0.70 ± 0.10	6.78 ± 0.08	–	II
Ser 44	II	7.6	1.36 ± 0.18	7.83 ± 0.25	9.08 ± 2.94	III
Asp 46	II	5.8	1.01 ± 0.36	5.48 ± 0.14	–	II
Ala 47	II	6.6	1.25 ± 0.31	6.88 ± 0.50	6.59 ± 0.49	III
Asp 48	II	5.5	0.48 ± 0.12	–	5.13 ± 0.08	I
Asn 50	II	8.2	1.97 ± 0.17	8.02 ± 0.09	–	II
Glu 52	II	7.6	1.18 ± 0.06	7.39 ± 0.07	–	II
Ala 59	II	9.9	2.91 ± 0.45	11.16 ± 0.75	–	II
Lys 78	III	6.3	1.09 ± 0.14	5.94 ± 0.10	–	II
Val 79	III	5.2	0.60 ± 0.09	5.50 ± 0.09	–	II
Leu 80	III	8.7	1.33 ± 0.19	9.24 ± 0.32	8.45 ± 0.16	III
Tyr 81	III	9.2	1.33 ± 0.24	9.870 ± 0.43	8.86 ± 0.17	III
Lys 82	III	7.8	0.96 ± 0.32	8.50 ± 0.57	8.14 ± 0.45	III
Val 86	III	5.9	0.54 ± 0.06	5.62 ± 0.05	–	II
Lys 91	III	ND[b]	0.93 ± 0.10	7.45 ± 0.12	–	II
Leu 92	III	6.0	0.56 ± 0.08	5.53 ± 0.10	–	II
Thr 93	III	7.4	1.22 ± 0.32	8.10 ± 0.69	6.61 ± 0.14	III
Val 97	III	8.6	1.29 ± 0.29	9.89 ± 0.58	8.18 ± 0.08	III
Thr 98	III	6.6	1.37 ± 0.45	9.62 ± 1.11	6.05 ± 0.02	III
Phe 100	III	6.4	0.18 ± 0.02	–	5.84 ± 0.02	I
Phe 101	III	ND[b]	0.99 ± 0.43	7.56 ± 0.84	6.48 ± 0.22	III
Lys 102	III	5.1	2.84 ± 1.06	6.02 ± 0.79	4.57 ± 0.16	III
Ala 118	IV	5.8	1.20 ± 0.14	5.38 ± 0.10	–	II
Asp 121	IV	6.6	1.98 ± 0.30	6.21 ± 0.15	–	II
Tyr 123	IV	ND[b]	1.20 ± 0.12	7.49 ± 0.15	–	II
Ile 124	IV	6.3	0.46 ± 0.07	5.65 ± 0.07		II
Glu 128	IV	5.2	0.20 ± 0.03	–	4.49 ± 0.04	I
Phe 129	IV	9.4	1.65 ± 0.05	9.37 ± 0.06	–	II
Leu 130	IV	7.2	1.04 ± 0.22	7.46 ± 0.47	6.49 ± 0.18	III

[a] The EF-hand location and the mechanism of unfolding are also shown. For classification of the unfolding mechanism, please see text. [b] ΔG_{HX} was not determined for those residues in the absence of denaturant due to very slow exchange kinetics.

state hydrogen exchange experiments in the EX2 regime as described in Materials and Methods. To ensure that the protein remains in the EX2 regime, we measured the k_{obs} with an increasing pH (Figure S1 of the Supporting Information). An increase in k_{obs} with pH or k_{rc} is direct evidence which confirms that the closure kinetic constant is much larger than the exchange rate ($k_{cl} \gg k_{rc}$) at the measured pH values and hence the EX2 mechanism. Evident in Figure S1 is the fact that the k_{obs} values for all the residues increase linearly with pH and the protein remains in the EX2 regime up to pH 9.0.

Measurement of Stabilization Free Energies. Native-state HX experiments were carried out on *Eh*CaBP at a pH of 7.0 as described in Materials and Methods. At this pH, many of the backbone $^1H^N$ resonances undergo fast deuterium kinetics. However, we could monitor the decay for 54 residues (of the 134 residues present in the protein) for which the k_{obs} was obtained by fitting the peak volumes to a single-exponential decay. The stabilization free energy of the individual residues (ΔG_{HX}) (Table 1) was calculated using eq 5, and ΔG_{HX} was plotted against the residue number (Figure 2). It is evident from Figure 2 that the protected residues belong to four different regions, which essentially correspond to the four EF-hands present in the protein. Moreover, there is a well-protected region of contiguous

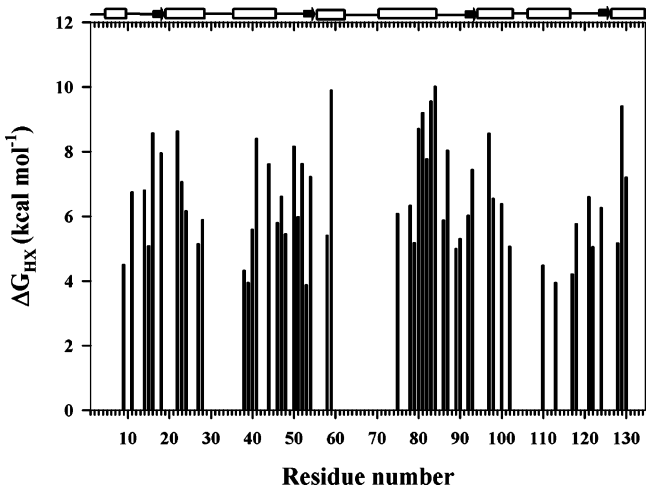

FIGURE 2: Free energies of unfolding (ΔG_{HX}) for all the residues measured plotted vs residue number. The secondary structural elements are shown schematically with arrows (β strands) and cylinders (α helix).

residues stretching from K78 to M84 having significant protection or ΔG_{HX}. Interestingly, this stretch corresponds to the longest helix present in the protein. This contiguous stretch could be a partially unfolded form (PUF) or might

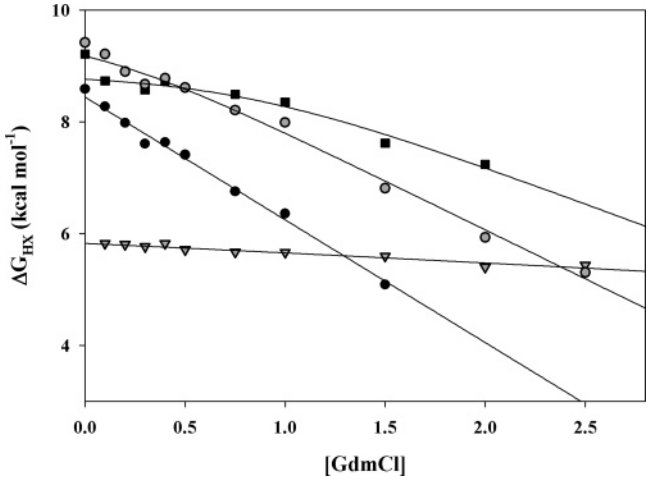

FIGURE 3: Illustrative examples for four representative backbone $^1H^N$ atoms [A16 (black circle), Y81 (square), F−100 (triangle), and F129 (gray circle)] showing the changes in free energy of HX (ΔG_{HX}) as a function of [GdmCl] in *Eh*CaBP.

be protected by some uncorrelated local fluctuations as discussed below.

Segregating the Local Fluctuations and Global Unfolding Phenomenon in EhCaBP. In many cases, backbone $^1H^N$ undergoes HX via a small local fluctuation mechanism which does not require the protein to undergo huge structural unfolding. The free energy of HX (ΔG_{HX}) measured above represents a combination of both the opening transitions, namely, the structural unfolding and local fluctuations. These mechanisms are different from one another; hence, it becomes essential to distinguish the mode of HX before interpreting the HX data. Evaluating the rates of exchange as a function of denaturant concentration such as GdmCl allows one to distinguish between these two processes (*29*, *39*). Addition of GdmCl promotes exposure of nonpolar surface area and therefore alters the equilibrium constant of unfolding. However, by definition, it does not affect local fluctuations that do not expose any extra nonpolar surface area and have fluctuation energies below those observed for global unfolding. Hence, the exchange that appears to be denaturant-independent is attributed to local fluctuations. With the addition of denaturant, the free energy of unfolding drops and the HX is dominated by the unfolding events.

In this study, the distinction between the contribution arising from local fluctuations and the global unfolding events to the HX exchange process for each residue in *Eh*CaBP was determined by performing a set of HX experiments at nine different GdmCl concentrations ranging from 0.1 to 2.5 M (under the subdenaturing condition), and the corresponding ΔG_{HX} values were obtained at all ten concentrations as discussed above using eq 5. The denaturant-dependent behaviors for four residues are shown in Figure 3. As seen in Figure 3, three different types of ΔG_{HX} profiles are noticed: (i) independence from [GdmCl], or a near-zero *m* value (HX for these residues occurs through local fluctuation), (ii) a linear dependence on [GdmCl] (the opening for this type is a cooperative unfolding event), and (iii) biphasic with a near-zero *m* value at low [GdmCl] values and a larger *m* value at higher [GdmCl] values. The free energy for this class of residues has the contributions arising from both local fluctuations and global unfolding (*39*). The individual contributions of the free energy of unfolding

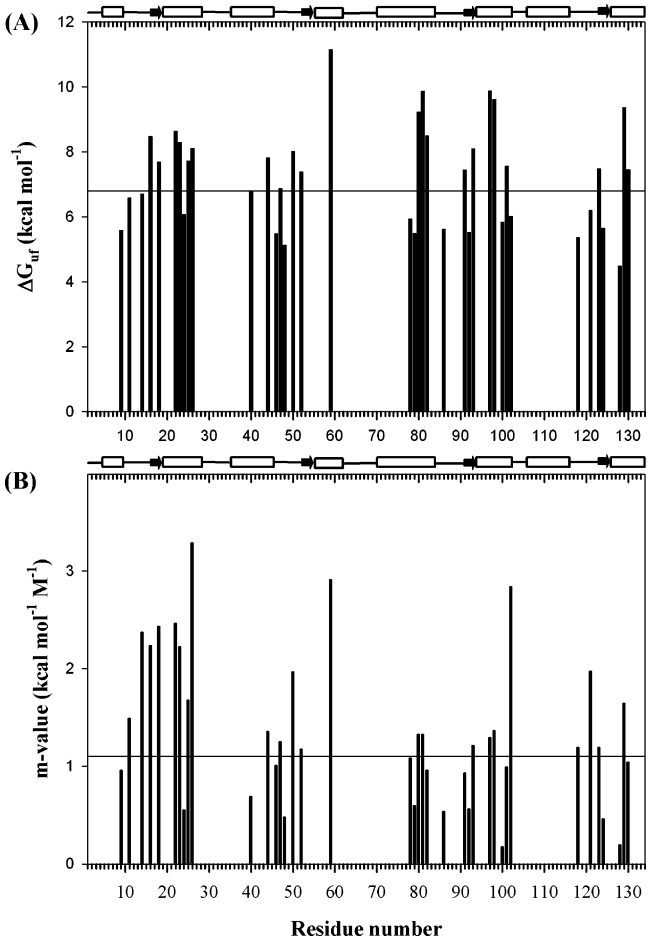

FIGURE 4: (A) Free energies of unfolding (ΔG_{uf}) and (B) *m* value plotted vs the primary sequence. Secondary structure is plotted over the graph by arrows (β strands) and cylinders (α helix). ΔG_{uf} and the *m* value for L83 and M84 could not be measured due to high level of protection of these residues. The average ΔG_{uf} by native-state HX is 7.2 kcal/mol with a standard deviation of 1.5 kcal/mol. The average *m* value for the protein as detected by native-state HX is 1.4 kcal mol^{-1} M^{-1} with a standard deviation of 0.8 kcal mol^{-1} M^{-1}. The horizontal solid line in panels A and B represents the ΔG_{uf} value and *m* value measured using CD spectroscopy.

(ΔG_{uf}) and free energy of local fluctuation (ΔG_{lf}) are segregated by fitting the curves to eq 6. The thermodynamic parameters thus obtained for each residue are listed in Table 1. Thus, these GdmCl experiments allowed us to distinguish between the EX2 mechanism and local fluctuations. On the basis of the ΔG_{HX} profiles that were obtained, each residue was thus assigned to one of the three above-mentioned classes (Table 1).

Panels A and B of Figure 4 show ΔG_{uf} and the corresponding *m* values, respectively, for *Eh*CaBP plotted against residue number. ΔG_{uf} could not be measured in the linkers connecting the EF-hands because of their rapid exchange due to their exposure to solvent and flexible nature. A summary of average ΔG_{uf} and *m* values for the individual EF-hands is provided in Table 2. Except for EF-hand IV, all the other EF-hands have similar average ΔG_{uf} values. The standard deviation of ΔG_{uf} gives an idea of the spread of ΔG_{uf} around the mean value. It is evident from the data (Table 2) that significant differences have been observed in their individual *m* values among the four EF-hands present in the protein. EF-hand I has the highest *m* values followed by EF-hands II and IV, which have similar *m* values, and

Table 2: Summary of ΔG_{uf} and *m* Values for the Four EF-Hands Present in *Eh*CaBP

EF-hand	no. of residues monitored	⟨*m* value⟩ (kcal mol^{-1} M^{-1})	standard deviation of the *m* value (kcal mol^{-1} M^{-1})	⟨ΔG_{uf}⟩ (kcal/mol)	standard deviation of ⟨ΔG_{uf}⟩ (kcal/mol)
I	10	2.0	0.8	7.4	1.1
II	8	1.4	0.8	7.3	1.9
III	13	1.0	0.4	7.2	1.7
IV	7	1.1	0.6	6.6	1.6

EF-hand III has the lowest *m* values. This suggests that the denaturant dependence is the highest for EF-hand I and lowest for EF-hand III. Although there are differences in the *m* values for all the EF-hands, we observed some novel features which are common to all EF-hands. For example, the residues at positions 13 and 14 that are part of the F-helices, namely, V−22, K−23, A−59, V−97, T−98, F−129, and F−130, undergo global unfolding with high ΔG_{uf} and *m* values (Table 1). The only exception is F58. In EF-hand CaBPs, the residue at position 13 belonging to the F-helix is highly conserved, which is predominantly aromatic or hydrophobic. The fact that the F-helices are initiated at position 10 of the Ca^{2+} binding loops suggests that the residues at position 13 are stabilized by a single hydrogen bond. In *Eh*CaBP, they are V22(CO) → V26(NH), F58(CO) → Y62(NH), V97(CO) → F101(NH), and F129(CO) → S133(NH). Earlier, it was also suggested that residue 13 of EF-hand II within a given domain (which is occupied by an aromatic residue, predominantly a Phe) comes into the proximity of residue −4 of EF-hand I in the same domain (which is also occupied by an aromatic/hydrophobic residue, again predominantly a Phe) of a CaBP such that the two aromatic rings are almost orthogonal to each other (*51*). On the other hand, the residues at position 14 are stabilized by two hydrogen bonds [e.g., A59(NH) → Q55(CO) and A59-(CO) → G63(NH) in EF-hand II of *Eh*CaBP]. In *Eh*CaBP, all these residues at positions 13 and 14 possess high energies of global unfolding, except the one at position 13 of EF-hand II (F58). Hence, these residues may be involved in a key role in terms of protein unfolding and folding of an EF-hand. Then the question of why F58 undergoes fast deuterium exchange arises. This could be possibly due to the hydrogen bond forming partner of F58 in EF-hand II which is Y62, while the corresponding partners are V26, F101, and S133 in EF-hands I, III, and IV, respectively. However, V, F, and S have a stronger propensity to form an α-helix than Y, which can be observed from the Chou−Fasman scale (*52*). Moreover, Y62 is followed by G63 which is a strong helix breaker. These could be the reasons for the fast deuterium exchange rate for F58.

DISCUSSION

Native Energy Landscape of EhCaBP

Evidence for the Presence of Intermediates in the Energy Landscape. The unfolding free energies (ΔG_{uf}) (Figure 4A) and the corresponding denaturation dependence (*m* values) (Figure 4B) for the measured residues are shown on the three-dimensional (3D) structure of the protein (Figure 5A,B). The unfolding experiment using CD spectroscopy yielded a lower ΔG_{uf} value (6.8 ± 0.3 kcal/mol) compared to those obtained for different residues from the HX study (Figure 4A), suggesting that these residues are superprotected during the unfolding process. Such superprotection is known to arise due to different factors such as cis−trans isomerization, bulk solvent effects, or the presence of intermediates (*34*). Considering the fact that *Eh*CaBP does not contain any Pro residue, the possibility of cis−trans isomerization leading to superprotection is ruled out. The far-UV CD experiments were carried out in ^2H_2O similar to that of HX experiments, and hence, a bulk solvent effect can also be ruled out. Therefore, the presence of intermediates in the folding pathway can only be a plausible reason which leads to the superprotection of various residues in the protein. Further, the low cooperativity of the unfolding transition monitored by CD spectroscopy (*m* value = 1.1 ± 0.1 kcal mol^{-1} M^{-1}) can also be attributed to the presence of transient intermediates in the unfolding pathway which in general leads to an underestimation of thermodynamic parameters such as ΔG_{uf} values (*53*).

The presence of intermediates in the unfolding transition is supported further by the following evidence. There exists a contiguous stretch of seven residues (K78−M84) in the C-terminal domain, which is highly protected and is a part of the longest helix in the protein (Figure 5A). This stretch comprises mainly hydrophobic residues. Incidentally, this stretch is relatively the most protected region in the Ca^{2+}-free form of the protein, too (*43*). Further, we observed the presence of three contiguous amino acid residues (L80−K82) with similar *m* and ΔG_{uf} values (Table 1). This indicates

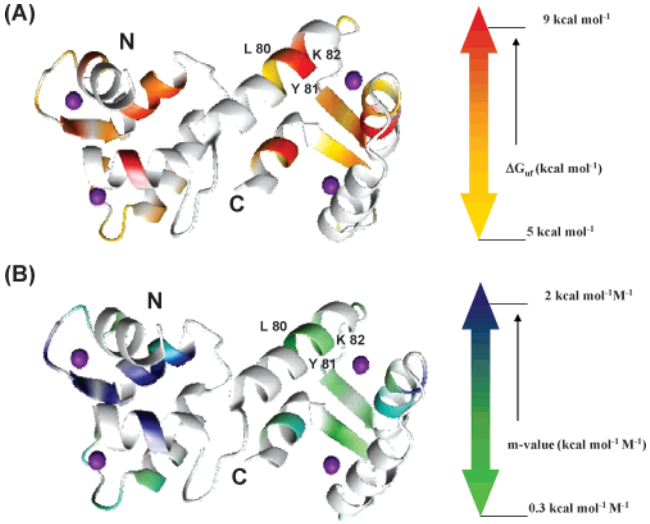

FIGURE 5: Distribution of free energies of unfolding (ΔG_{uf}) (A) and *m* values (B) for the residues measured in *Eh*CaBP shown on the 3D structure of the protein (PDB entry 1jfk). Individual residues are colored according to their ΔG_{uf} and *m* values determined by HX. Residues corresponding to the cooperative unfolding unit (L80−K82) are labeled. The image was produced using MolMol (*55*).

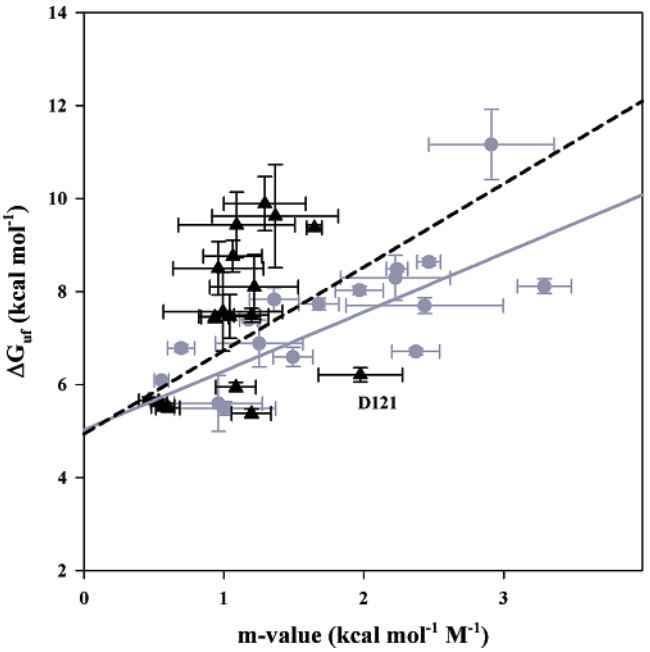

FIGURE 6: Calculated free energies of unfolding (ΔG_{uf}) plotted vs the corresponding *m* values for all measured amide protons. Stronger GdmCl concentration dependence in terms of *m* value is observed for residues corresponding to the N-terminal domain residues (gray circles) as compared to the C-terminal domain residues (triangles). The linearity between ΔG_{uf} and *m* values for both domains is also shown with a solid line (N-terminal) and a dashed line (C-terminal). A linear dependence was observed between the free energy of unfolding and *m* values for the N-terminal domain residues (gray solid line). The outlier residue of the C-terminal domain (D−121) is labeled.

that L80−K82 may act as a cooperative folding unit and hence a PUF (*37*). The isotherms for these residues are shown in Figure S2 of the Supporting Information. On the other hand, there exists a contiguous stretch of five residues (V22−V26) in the N-terminal domain, which undergoes global unfolding. However, the ΔG_{uf} and the *m* value are not same for this entire stretch (Table 1). Besides, this stretch is not protected in the Ca^{2+}-free form of the protein (*43*), indicating that the stability of this stretch is associated with metal binding. Thus, it is evident from the data that *Eh*CaBP unfolds cooperatively via intermediates and the three-residue PUF (L80−K82) identified in the C-terminal domain.

Distinct Folding Features of N- and C-Terminal Domains. In earlier studies (*29*), a linear correlation was observed between ΔG_{uf} and *m* value. However, in this study, the observed ΔG_{uf} and *m* value of individual residues corresponding to the two domains of *Eh*CaBP cluster separately (Figure 6). We observed a linear correlation between the ΔG_{uf} and *m* values among the residues belonging to the N-terminal domain. However, corresponding values for the residues in the C-terminal domain are found clustered with greater variation in ΔG_{uf} values but with a narrow range of *m* values of 1 kcal mol^{-1} M^{-1} (Figure 5B), indicating a range of ΔG_{uf} values with less denaturant dependence. Besides, there are residues having lower ΔG_{uf} values at a near-zero *m* value. D121 is an exception to this trend observed in the C-terminal domain. From the observation described above, it can be concluded that though the average stability of each of the domains is similar in terms of ΔG_{uf}, the folding landscape comprises of discrete intermediates rather than a continuum when *m* values are compared with respect to their respective ΔG_{uf}. All these observations taken together establish that the two domains in *Eh*CaBP have distinct folding features. Further, from the data (Table 2), it is clear that the N-terminal domain which has a higher *m* value undergoes HX via global unfolding while the C-terminal domain undergoes HX via local fluctuations to a large extent. In fact, one can conclude that the conformational and/or local fluctuations present in the C-terminal domain can act as nucleation sites (*54*) for the formation of small cooperative unfolding units, as observed here, through which the domain unfolds.

Implications for the Structure Folding and Function Paradigm of Calcium Sensor Proteins. The study of the native energy landscape of *Eh*CaBP described here has major implications for our understanding of the functional aspects of calcium sensor proteins, which undergo huge conformational changes upon binding Ca^{2+} first and then various other target sequences (*10*, *16*, *24*). From the results described above, it is clear that the unfolding of N- and C-terminal domains has distinct folding features in spite of the fact that both of them contain two EF-hands each. Since the C-terminal domain is dominated by the local fluctuations, which is evident from the low *m* values (Figure 4B), it can be predicted that the C-terminal domain is more susceptible to readjustment of its conformation during the target binding. In fact, these tuned or cooperative motions are essential for changing the conformation according to the demand of the target molecules to bind and carry out various signal transduction processes.

CONCLUDING REMARKS

EF-hand proteins from the Ca^{2+} sensor family are known to undergo conformational changes upon binding to target sequences apart from the conformational changes that they undergo upon binding to Ca^{2+}. From this study of the HX process, we could describe the native energy landscape of *Eh*CaBP, which is essential for understanding the structure-folding and function paradigm of calcium sensor proteins. It is observed that the two domains in this protein have distinct folding features with respect to each other. The N-terminal domain is dominated with global unfolding events, which is evidenced by the large denaturant dependence, whereas the C-terminal domain is dominated by the local fluctuations and also unfolds in a more cooperative manner. A cooperative unfolding unit involving the longest helix in the protein is observed during the unfolding study, thereby leading to the conclusion that the unfolding of *Eh*CaBP comprises intermediates and is not a two-state process as observed by conventional experiments. Further, these observed differences in folding features of N- and C-terminal domains of a calcium sensor protein would have implications for domain-dependent target recognition.

ACKNOWLEDGMENT

We thank Prof. Alok Bhattacharya (JNU, New Delhi, India) for providing the *Eh*CaBP clone.

SUPPORTING INFORMATION AVAILABLE

Representative plots of experimentally determined k_{obs} values versus pH for a few selected residues (Figure 1S)

and changes in the free energy of HX (ΔG_{HX}) as a function of [GdmCl] in *Eh*CaBP for the backbone $^1H^N$ in the cooperative unfolding unit (Figure 2S). This material is available free of charge via the Internet at http://pubs.acs.org.

REFERENCES

1. D'Ascenzo, M., Piacentini, R., Casalbore, P., Budoni, M., Pallini, R., Azzena, G. B., and Grassi, C. (2006) Role of L-type Ca^{2+} channels in neural stem/progenitor cell differentiation, *Eur. J. Neurosci. 23*, 935−944.
2. Rizzuto, R., and Pozzan, T. (2006) Microdomains of intracellular Ca^{2+}: Molecular determinants and functional consequences, *Physiol. Rev. 86*, 369−408.
3. Dreval, V., Dieterich, P., Stock, C., and Schwab, A. (2005) The role of Ca^{2+} transport across the plasma membrane for cell migration, *Cell. Physiol. Biochem. 16*, 119−126.
4. Feranchak, A. P., Doctor, R. B., Troetsch, M., Brookman, K., Johnson, S. M., and Fitz, J. G. (2004) Calcium-dependent regulation of secretion in biliary epithelial cells: The role of apamin-sensitive SK channels, *Gastroenterology 127*, 903−913.
5. Wray, S., Jones, K., Kupittayanant, S., Li, Y., Matthew, A., Monir-Bishty, E., Noble, K., Pierce, S. J., Quenby, S., and Shmygol, A. V. (2003) Calcium signaling and uterine contractility, *J. Soc. Gynecol. Invest. 10*, 252−264.
6. Berridge, M. J., Bootman, M. D., and Lipp, P. (1998) Calcium: A life and death signal, *Nature 395*, 645−648.
7. Denecker, G., Vandenabeele, P., Grooten, J., Penning, L. C., Declercq, W., Beyaert, R., Buurman, W. A., and Fiers, W. (1997) Differential role of calcium in tumour necrosis factor-mediated apoptosis and secretion of granulocyte-macrophage colony-stimulating factor in a T cell hybridoma, *Cytokine 9*, 631−638.
8. Heizmann, C. W. (1993) Calcium signaling in the brain, *Acta Neurobiol. Exp. 53*, 15−23.
9. Heizmann, C. W., and Schafer, B. W. (1990) Internal calcium-binding proteins, *Semin. Cell Biol. 1*, 277−282.
10. Bhattacharya, S., Bunick, C. G., and Chazin, W. J. (2004) Target selectivity in EF-hand calcium binding proteins, *Biochim. Biophys. Acta 1742*, 69−79.
11. Ababou, A., and Desjarlais, J. R. (2001) Solvation energetics and conformational change in EF-hand proteins, *Protein Sci. 10*, 301−312.
12. Nelson, M. R., and Chazin, W. J. (1998) Structures of EF-hand Ca^{2+}-binding proteins: Diversity in the organization, packing and response to Ca^{2+} binding, *Biometals 11*, 297−318.
13. Heizmann, C. W. (1992) Calcium-binding proteins: Basic concepts and clinical implications, *Gen. Physiol. Biophys. 11*, 411−425.
14. Kretsinger, R. H., and Nockolds, C. E. (1973) Carp muscle calcium-binding protein. II. Structure determination and general description, *J. Biol. Chem. 248*, 3313−3326.
15. Strynadka, N. C., and James, M. N. (1989) Crystal structures of the helix-loop-helix calcium-binding proteins, *Annu. Rev. Biochem. 58*, 951−998.
16. Finn, B. E., Evenas, J., Drakenberg, T., Waltho, J. P., Thulin, E., and Forsen, S. (1995) Calcium-induced structural changes and domain autonomy in calmodulin, *Nat. Struct. Biol. 2*, 777−783.
17. Hanley, J. G., and Henley, J. M. (2005) PICK1 is a calcium-sensor for NMDA-induced AMPA receptor trafficking, *EMBO J. 24*, 3266−3278.
18. Hilge, M., Aelen, J., and Vuister, G. W. (2006) Ca^{2+} regulation in the Na^+/Ca^{2+} exchanger involves two markedly different Ca^{2+} sensors, *Mol. Cell 22*, 15−25.
19. Shaw, G. S., Hodges, R. S., and Sykes, B. D. (1990) Calcium-induced peptide association to form an intact protein domain: ^1H NMR structural evidence, *Science 249*, 280−283.
20. Vinogradova, M. V., Stone, D. B., Malanina, G. G., Karatzaferi, C., Cooke, R., Mendelson, R. A., and Fletterick, R. J. (2005) Ca^{2+}-regulated structural changes in troponin, *Proc. Natl. Acad. Sci. U.S.A. 102*, 5038−5043.
21. Hackney, C. M., Mahendrasingam, S., Penn, A., and Fettiplace, R. (2005) The concentrations of calcium buffering proteins in mammalian cochlear hair cells, *J. Neurosci. 25*, 7867−7875.
22. Lambers, T. T., Mahieu, F., Oancea, E., Hoofd, L., de Lange, F., Mensenkamp, A. R., Voets, T., Nilius, B., Clapham, D. E., Hoenderop, J. G., and Bindels, R. J. (2006) Calbindin-D28K dynamically controls TRPV5-mediated Ca^{2+} transport, *EMBO J. 25*, 2978−2988.
23. Rosenbaum, E. E., Hardie, R. C., and Colley, N. J. (2006) Calnexin is essential for rhodopsin maturation, Ca^{2+} regulation, and photoreceptor cell survival, *Neuron 49*, 229−241.
24. Nelson, M. R., and Chazin, W. J. (1998) An interaction-based analysis of calcium-induced conformational changes in Ca^{2+} sensor proteins, *Protein Sci. 7*, 270−282.
25. Dill, K. A., and Chan, H. S. (1997) From Levinthal to pathways to funnels, *Nat. Struct. Biol. 4*, 10−19.
26. Dobson, C. M., and Karplus, M. (1999) The fundamentals of protein folding: Bringing together theory and experiment, *Curr. Opin. Struct. Biol. 9*, 92−101.
27. Dyson, H. J., and Wright, P. E. (2005) Elucidation of the protein folding landscape by NMR, *Methods Enzymol. 394*, 299−321.
28. Bai, Y. (2003) Hidden intermediates and levinthal paradox in the folding of small proteins, *Biochem. Biophys. Res. Commun. 305*, 785−788.
29. Llinas, M., Gillespie, B., Dahlquist, F. W., and Marqusee, S. (1999) The energetics of T4 lysozyme reveal a hierarchy of conformations, *Nat. Struct. Biol. 6*, 1072−1078.
30. Mayne, L., and Englander, S. W. (2000) Two-state vs. multistate protein unfolding studied by optical melting and hydrogen exchange, *Protein Sci. 9*, 1873−1877.
31. Jackson, S. E. (1998) How do small single-domain proteins fold? *Folding Des. 3*, R81−R91.
32. Bollen, Y. J., Kamphuis, M. B., and van Mierlo, C. P. (2006) The folding energy landscape of apoflavodoxin is rugged: Hydrogen exchange reveals nonproductive misfolded intermediates, *Proc. Natl. Acad. Sci. U.S.A. 103*, 4095−4100.
33. Englander, S. W. (2000) Protein folding intermediates and pathways studied by hydrogen exchange, *Annu. Rev. Biophys. Biomol. Struct. 29*, 213−238.
34. Huyghues-Despointes, B. M., Pace, C. N., Englander, S. W., and Scholtz, J. M. (2001) Measuring the conformational stability of a protein by hydrogen exchange, *Methods Mol. Biol. 168*, 69−92.
35. Krishna, M. M., Hoang, L., Lin, Y., and Englander, S. W. (2004) Hydrogen exchange methods to study protein folding, *Methods 34*, 51−64.
36. Arrington, C. B., and Robertson, A. D. (1997) Microsecond protein folding kinetics from native-state hydrogen exchange, *Biochemistry 36*, 8686−8691.
37. Bai, Y., Sosnick, T. R., Mayne, L., and Englander, S. W. (1995) Protein folding intermediates: Native-state hydrogen exchange, *Science 269*, 192−197.
38. Englander, S. W. (1998) Native-state HX, *Trends Biochem. Sci. 23*, 378−381.
39. Yan, S., Kennedy, S. D., and Koide, S. (2002) Thermodynamic and kinetic exploration of the energy landscape of *Borrelia burgdorferi* OspA by native-state hydrogen exchange, *J. Mol. Biol. 323*, 363−375.
40. Chamberlain, A. K., Handel, T. M., and Marqusee, S. (1996) Detection of rare partially folded molecules in equilibrium with the native conformation of RNaseH, *Nat. Struct. Biol. 3*, 782−787.
41. Bhattacharya, A., Padhan, N., Jain, R., and Bhattacharya, S. (2006) Calcium-binding proteins of *Entamoeba histolytica*, *Arch. Med. Res. 37*, 221−225.
42. Atreya, H. S., Sahu, S. C., Bhattacharya, A., Chary, K. V., and Govil, G. (2001) NMR derived solution structure of an EF-hand calcium-binding protein from *Entamoeba Histolytica*, *Biochemistry 40*, 14392−14403.
43. Mukherjee, S., Kuchroo, K., and Chary, K. V. (2005) Structural characterization of the apo form of a calcium binding protein from *Entamoeba histolytica* by hydrogen exchange and its folding to the holo state, *Biochemistry 44*, 11636−11645.
44. Hvidt, A., and Nielsen, S. O. (1966) Hydrogen exchange in proteins, *Adv. Protein Chem. 21*, 287−386.
45. Linderstrøm-Lang, K. (1958) *Symposium on Protein Structure*, pp 23−24, London.
46. Sahu, S. C., Bhattacharya, A., Chary, K. V., and Govil, G. (1999) Secondary structure of a calcium binding protein (CaBP) from *Entamoeba histolytica*, *FEBS Lett. 459*, 51−56.
47. Santoro, M. M., and Bolen, D. W. (1988) Unfolding free energy changes determined by the linear extrapolation method. 1. Unfolding of phenylmethanesulfonyl α-chymotrypsin using different denaturants, *Biochemistry 27*, 8063−8068.
48. Kay, L. E., Keifer, P., and Saarinen, T. (1992) Pure absorption gradient enhanced heteronuclear single quantum correlation spectroscopy with improved sensitivity, *J. Am. Chem. Soc. 114*, 10663−10665.

49. Bai, Y., Milne, J. S., Mayne, L., and Englander, S. W. (1993) Primary structure effects on peptide group hydrogen exchange, *Proteins 17*, 75−86.
50. Makhatadze, G. I., Clore, G. M., and Gronenborn, A. M. (1995) Solvent isotope effect and protein stability, *Nat. Struct. Biol. 2*, 852−855.
51. Rashidi, H. H., Bauer, M., Patterson, J., and Smith, D. W. (1999) Sequence motifs determine structure and Ca^{2+}-binding by EF-hand proteins, *J. Mol. Microbiol. Biotechnol. 1*, 175−182.
52. Chou, P. Y., and Fasman, G. D. (1978) Empirical predictions of protein conformation, *Annu. Rev. Biochem. 47*, 251−276.
53. Kamal, J. K., Nazeerunnisa, M., and Behere, D. V. (2002) Thermal unfolding of soybean peroxidase. Appropriate high denaturant concentrations induce cooperativity allowing the correct measurement of thermodynamic parameters, *J. Biol. Chem. 277*, 40717−40721.
54. Baxter, N. J., Hosszu, L. L., Waltho, J. P., and Williamson, M. P. (1998) Characterisation of low free-energy excited states of folded proteins, *J. Mol. Biol. 284*, 1625−1639.
55. Koradi, R., Billeter, M., and Wuthrich, K. (1996) MOLMOL: A program for display and analysis of macromolecular structures, *J. Mol. Graphics 14*, 32−51.

BI700477H